

Dynamometer Test Rig Drive Train Control with a High Dynamic Performance: Measurements and Experiences

Mohsen Neshati, Jan Wenske

*Fraunhofer Institute for Wind Energy Systems (IWES),
Dynamic Nacelle Laboratory, 27572 Bremerhaven, Germany.
(e-mail: mohsen.neshati@iwes.fraunhofer.de)*

Abstract: This paper presents the control design and dynamic performance evaluation for a 10 MW dynamometer test rig for wind turbine nacelles. The purpose is to control the applied torque by the drive train, required for an accurate emulation of rotor characteristics in the laboratory. This is implemented in a hardware-in-the-loop simulation framework for electrical certification test procedures, introducing high dynamic requirements. Therefore, a feedback-feedforward as well as a H-infinity controller is implemented to benefit from high dynamic and robustness capabilities, respectively. Furthermore, due to the lack of a suitable torque measurement in the meganewton-meter range, model-based algorithms are incorporated and the implemented time-varying Kalman filter provides the unmeasured variables. In addition, for performance analysis independent of any specimen, experiments using small signal perturbation as test functions are executed under load conditions. The results are analysed here elaborately and the obtained control bandwidth is distinguished under realistic conditions. Overall, the measurements demonstrate an effective control with a bandwidth of up to 30 Hz.

Keywords: Dynamometers, Automatic control, H-infinity control, Feedforward control, Kalman filters, Torque control, Dynamic tests, Dynamic properties, Hardware-in-the-loop simulation.

1. INTRODUCTION

Dynamometer ground test stands are an alternative to field tests for system validation and certification of wind energy converters (WEC) in the laboratory, under adjustable and repeatable load conditions. Here is a realistic environment by the means of Hardware-in-the-Loop (HiL) test methods provided, incorporating real-time simulation models emulating missing system components. Dynamic Nacelle Laboratory (DyNaLab) has been developed by Fraunhofer IWES in Bremerhaven, Germany, for testing WECs up to 10 MW. Main system components are illustrated in the schematic in Fig.1, enabling emulation of rotor torque as well as non-torque loads in overall six degrees of freedom (DOF). Furthermore, an inverter-based artificial grid supplies the device under test (DUT) and is capable of simulating various grid events.

Since inauguration of DyNaLab in 2015, seven DUTs from five different manufacturers in the range of 2.5 to 9 MW have been subject to extensive tests at DyNaLab. This demonstrates how beneficial system test benches are for manufacturers. However, comparison of test results with measurements obtained in the field is a necessary intermediate step to evaluate the validity and therefore further increase the acceptance also among certification authorities. In fact, this is the main topic of the research project CertBench, considering electrical certification test procedures (see Jassmann et al. (2019) and Neshati et al. (2019)). This project is a collaboration with the Center for Wind Power Drives (CWD) at RWTH university, and

Enercon GmbH, in form of a consortium including also certification bodies among others. For validation purposes, the Enercon E-115 E2 would be subject to electrical tests on both test rigs at IWES and CWD, considering national and international certification guidelines (see FGW (2018) and IEC (2019)). Development of HiL test methods with the required test rig control system, implementation of an adequate real-time WEC simulation tool, and execution of valid grid events are here among important tasks. In this context, a DUT is the intersection of mechanical and power HiL systems in the laboratory and therefore for the mutual interaction between rotor side dynamics and grid side events to be complete, only a minimal influence of test rig's own actuators is desired.

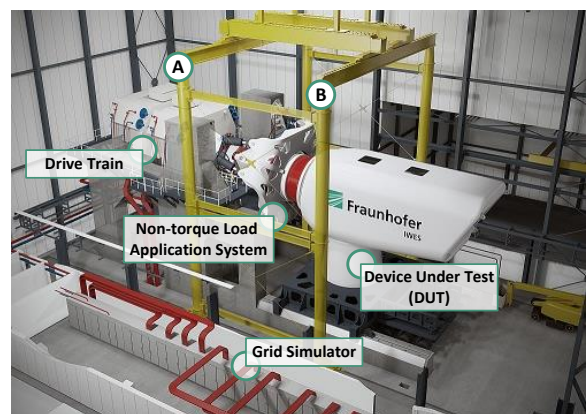


Fig. 1. Illustrative scheme of Dynamic Nacelle Laboratory

In this regard, an experimental evaluation of the drive train control performance at DyNaLab is presented here, accomplished by means of exclusive tests under load conditions and independent of any specific DUT. Furthermore, the control design and implementation is described including a clarification of the corresponding objective. In fact, this paper reveals for the first time the investigation on stability and accuracy issues based on measurements obtained from generic experiments. This includes examination of the mutual interaction between active control loops in different layers on both the test rig as well as the DUT side. Based on these, this paper describes details on performance measures of the full-scale nacelle test rig and distinguishes corresponding challenges for control design. A principal study on this topic is presented in Fischer and Jassmann (2017), clarifying the issue in theory for both power and mechanical HiL systems. Furthermore, a comprehensive introduction to the mechanical HiL system including control design is presented by Fischer et al. (2016), with the corresponding simulation results. Among other operational test rigs, Leisten et al. (2018) presents experimental results with a research DUT at CWD including the control design, and Schkoda et al. (2016) reports HiL testing activities at the National Renewable Energy Laboratory (NREL) and Clemson University. Furthermore, HiL testing for the purpose of controller validation is presented by Jassmann (2018).

1.1 System components

The drive train primary actuators are two synchronous and externally excited motors delivering a total nominal power of 10 MW in a tandem configuration (see Fig.2). Due to the direct drive machines and the unique design of drive train illustrated in Fig.3, torque could be applied with high dynamics having a nominal value of 8600 kNm. The drive system provides an overload capacity of up to 150% which is applicable over the complete operation range with a nominal speed of 11 rpm. In this context, the overriding drive train controller for HiL test purposes is implemented on the Power Electronic Controller (PEC) from ABB, providing a real-time platform with fast communication with the drive for set-point commanding and measurement feedbacks. On the other hand, the inverter-based grid simulator in operation has a short circuit capacity of 44 MVA. It is capable of symmetric and asymmetrical fault simulations, as well as voltage dips and frequency changes. Furthermore, different grid conditions are realized by an emulation of grid impedance.



Fig. 2. Synchronous drives coupled with a tandem shaft

2. OBJECTIVE

2.1 Control objective

With respect to the rotational DOF, it is desired to emulate rotor characteristics by means of the HiL framework introduced in Neshati et al. (2016). This is to enable comparable results with those from field tests by maintaining a realistic active power being delivered to the flange (point B in Fig.1). Among various approaches referenced in section 1, drive train torque control has been considered here by the authors to enable high dynamics, as well as consistency with the WEC controller that adjusts the speed and governs the overall system operation. This control is to be referred to as HiL controller further in this text. Furthermore, a sensor-less approach is required here, since a suitable torque measurement for control purpose in this range is not available (see Zhang et al. (2020)). In this context, this is the virtual rotor that provides the corresponding rotor response, being the set-points for system operation based on the input wind field, pitch, and an actual measurement feedback from the hardware. Virtual rotor is based on the aeroelastic WEC simulation tool MoWiT developed at IWES (see Feja and Huhn (2019)). Duty of the HiL controller is yet to follow and maintain the commanded set-point at the flange, during static as well as dynamic conditions. This includes not only the rotor side induced dynamics due to the stochastic wind field, aeroelastic rotor and the tower, but also grid transient events, all influencing system response simultaneously.

2.2 Back-to-back experimental set-up

Grid events are executed for certification test procedures as prescribed in the guidelines. These also define the required response of DUT to events such as frequency change or voltage dips, often resulting in a dramatic change of the active power. However, due to the small inertia of drive train in comparison with that of the rotor, and inherent dynamic of the underlying drive, response of the system in the laboratory could be impaired during mentioned transient events. Therefore, it is necessary to distinguish the plausible control bandwidth in the presence of dead-times, underlying drive dynamic and the additional HiL control loop, under realistic load conditions. For this reason, tests in a back-to-back configuration have been performed at DyNaLab where the second machine (M2) drives the system, and the first machine (M1) operates as a generator. Only in this way, system performance could be evaluated



Fig. 3. Torque limiter, flexible coupling, moment bearing

experimentally under load conditions, independent of any DUT. This enables tests under ideal conditions during which, maximum possible dynamic capability of the system is identified. For these tests, torsional torque of the tandem shaft is the controlled output (point A in Fig.1), since only this coupling is under load. The rest of the drive train up to the flange (point B in Fig.1) would rotate with no-load in this case.

3. CONTROL SYNTHESIS

This section describes the state-space controllers implemented, as well as the Kalman filter providing an estimation of the unmeasured output and state-variables. The control block diagram in Fig.4 illustrates the back-to-back configuration without the presence of any DUT. Actuating variable in this case is m_a designating air-gap torque of the motor (M2), whereas m_g denotes that of the generator (M1) as a measured disturbance. In this configuration, torsional torque of the tandem shaft is the controlled output denoted by m_t , however, this changes to the flange torque (m_{fl}) during a complete test with a commercial DUT. Furthermore, ω assigns angular velocity and the superscripts * and $\hat{}$ indicate a set-point and an estimation of the corresponding measure, respectively. The described configuration allows testing under load over the complete range in a variable torque and speed operation mode, enabling simulation of WEC operation in the partial as well as full-load region. The controller is designed in discrete time using MATLAB and implemented in real-time on the PEC hardware, executed finally with a sample time of $250 \mu s$. For control synthesis in the following, consider the plant state-space model below, where \mathbf{A} is the system matrix, B , E , C are input and output vectors, and X is the corresponding state-variable vector.

$$\begin{cases} \dot{X}(t) = \mathbf{A} X(t) + B m_a(t) + E m_g(t) \\ m_t(t) = C X(t) \end{cases} \quad (1)$$

3.1 Feedback-Feedforward Controller

Here a Linear Quadratic Regulator is implemented, providing a feedback-feedforward structure with the advantage of a fast disturbance rejection, held to be important for this application. This controller with the straightforward design is implemented as a benchmark for further comparison, leading to the following closed-loop state-space model

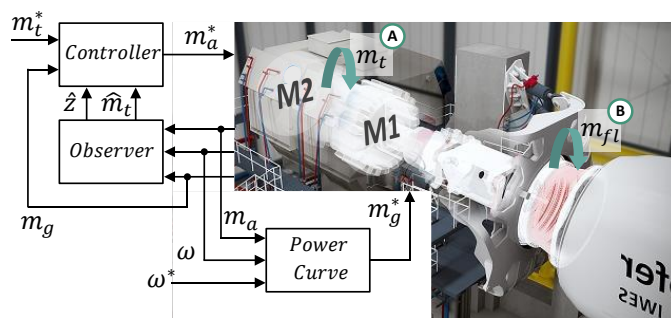


Fig. 4. Control block diagram in the back-to-back test configuration

$$\begin{cases} \dot{X}(t) = (\mathbf{A} - B K) X(t) + v B m_a^*(t) + (f B + E) m_g(t) \\ m_t(t) = C X(t). \end{cases} \quad (2)$$

K designates the static feedback vector, v and f correspond to the pre-filter and feedforward gain, respectively, as defined below

$$v = (-C(\mathbf{A} - B K)^{-1} B)^{-1}, f = -v(-C(\mathbf{A} - B K)^{-1} E). \quad (3)$$

3.2 H-infinity Robust Controller

In order to take advantage of controller design in frequency domain, a H-infinity robust controller is implemented here incorporating the mixed sensitivity approach. This is done with a reformulation of the control problem, by augmenting the plant including additional sensitivity transfer functions. This leads to the following state-space representation of the augmented plant,

$$\begin{cases} X_a(t) = \mathbf{A}_a X_a(t) + \mathbf{B}_{a1} W(t) + \mathbf{B}_{a2} U(t) \\ Z(t) = \mathbf{C}_{a1} X_a(t) + \mathbf{D}_{a11} W(t) + \mathbf{D}_{a12} U(t) \\ Y(t) = \mathbf{C}_{a2} X_a(t) + \mathbf{D}_{a21} W(t) + \mathbf{D}_{a22} U(t) \end{cases} \quad (4)$$

with the corresponding variables as defined for (1), where the subscript a denotes to the augmented plant \mathbf{P} . In addition, \mathbf{D}_a is the feed-through matrix, and U designates the manipulating input vector. Furthermore, W defines the exogenous input vector, while Z represents vector of the penalty function. Y here is the output vector of the augmented system. Subsequently, for control design, an optimization problem is defined minimizing the transfer function from W to Z , while shaping the sensitivity and complementary sensitivity functions as well as the actuating variable response. In this sense, system equation in (4) is reformulated as below,

$$\begin{pmatrix} Z(s) \\ Y(s) \end{pmatrix} = \begin{pmatrix} \mathbf{P}_{11}(s) & \mathbf{P}_{12}(s) \\ \mathbf{P}_{21}(s) & \mathbf{P}_{22}(s) \end{pmatrix} \begin{pmatrix} W(s) \\ U(s) \end{pmatrix} \quad (5)$$

where \mathbf{P}_{ij} includes the corresponding transfer function of \mathbf{P} . Finally, a target transfer function is defined as below,

$$\mathcal{F}(\mathbf{P}, \mathbf{K}) = \frac{Z(s)}{W(s)} = \mathbf{P}_{11} + \mathbf{P}_{12} \mathbf{K} (\mathbf{I} - \mathbf{P}_{22} \mathbf{K})^{-1} \mathbf{P}_{21} \quad (6)$$

to be optimized while being influenced by the plant \mathbf{P} as well as the controller \mathbf{K} . Finally, the controller is obtained by the solution to the defined problem using linear matrix inequalities (LMI). For more details on control design see Neshati et al. (2017).

3.3 Discrete Kalman Filter

For an effective estimation of the unmeasured variables, a discrete time-varying Kalman filter is designed and implemented. This is an effective optimal estimator that provides robustness in the presence of noise, since stochastic properties of noisy measurements and plant model perturbations are taken in to account during the design. For the design, a plant model similar to (1) is formed and further augmented as below, where W_b and n represent the process and measurement noise, respectively. \mathbf{G}_b is incorporated here to define stochastic properties for each individual

$$\begin{cases} \dot{X}_b(t) = \mathbf{A}_b X_b(t) + \mathbf{B}_b U_b(t) + \mathbf{G}_b W_b(t) \\ y(t) = \mathbf{C}_b X_b(t) + n(t) \end{cases} \quad (7)$$

internal state. The plant model used here for observer design includes the system matrix A_b , input and output vectors B_b and C_b , respectively. The corresponding state variable vector is X_b and U_b defines input vector of the filter, being ω , m_a , and m_g . For the discrete filter design, an observer gain $L[k]$ is calculated as in (8), as a result of an optimization process minimizing steady-state of the error covariance matrix P_b . Here, R_{kal} corresponds to the magnitude of covariance of measurement noise. Finally, the time-varying filter is implemented by two recursive processes taking place iteratively, namely, the correction and progress processes.

$$L[k] = \frac{P_b[k|k-1]C_b^T}{C_b P_b[k|k-1]C_b^T + R_{kal}} \quad (8)$$

4. EXPERIMENTS AND RESULTS

For a complete evaluation of the control performance, experiments under static as well dynamic conditions have been designed. These have been accomplished using the back-to-back configuration described in section 2.2 as illustrated in Fig.4. This section provides a description of each test case and presents the results with an analysis.

4.1 Static tests

This defines a set of experiments where variable torque levels have been applied during constant speed operation, over the complete torque and speed range. During these tests, commissioning and tuning of the controller and observer system have been completed in the first place. Fig.5 illustrates the result at a constant nominal speed, where torque is stepwise increased up to 100%. This is to investigate control performance in terms of steady-state accuracy. Measurement results over the complete operating range demonstrate a high steady-state accuracy independent of the working point. Furthermore, it has been determined that drive limitations in terms of torque rate or absolute value remain constant and the system experiences a linear operation. The correlation between estimated torque and the actual measure is out of the scope of this paper. However, this is to be evaluated during tests with a DUT having a pre-defined power curve.

4.2 Dynamic Tests

In order to identify system dynamic response, a set of experiments have been designed and accomplished including application of small signal perturbations to the system

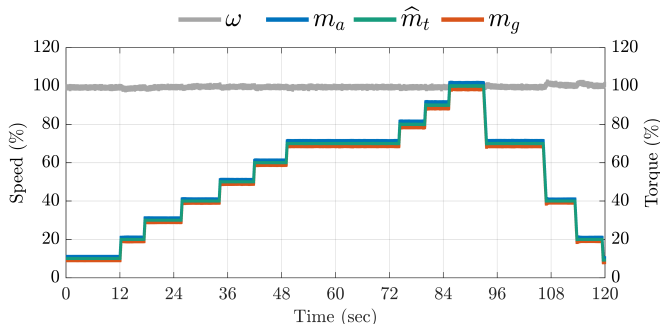


Fig. 5. Static operation (constant speed - variable torque)

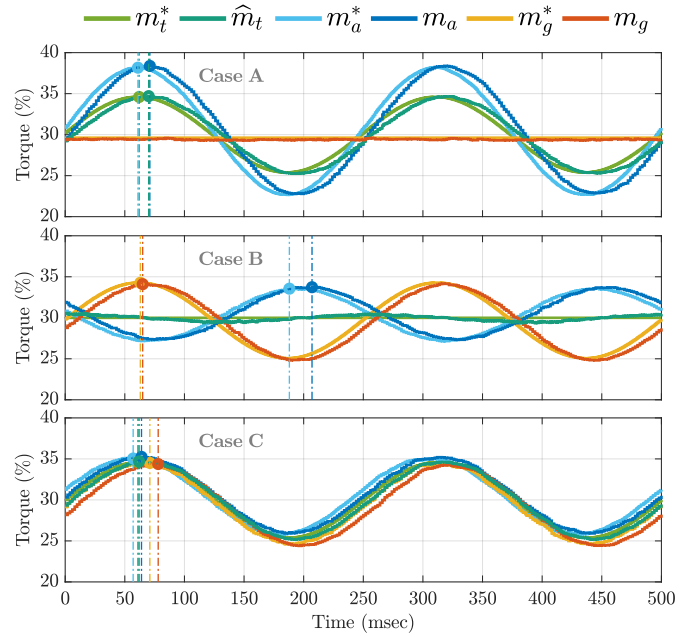


Fig. 6. Small signal perturbation tests at 4 Hz

under load conditions during constant speed operation. The perturbation signal here is applied in terms of torque being exerted as the reference (m_t^*) or as the disturbance (m_g^*), as well as both cases simultaneously. Therefore, overall three different test cases have been accomplished as defined below. For each, perturbations have been applied with a magnitude of 5% at the constant operating point of 30% torque, in a frequency range between 1 to 40 Hz. Fig.6 elaborates this set of experiment with an example measurement at a frequency of 4 Hz.

- *Dynamic reference torque setting during constant load (Case A)*: This is to elaborate reference following performance of the closed loop system, at the ideal condition of a constant disturbance independent of any torque or speed perturbations. The ratio between maximum of m_a and m_t in this case is due to inertia compensation for $M2$.
- *Dynamic load application during a constant reference torque (Case B)*: This test case demonstrates disturbance rejection performance of the closed loop system. Here, the controller is to compensate disturbance perturbation by generating the corresponding counter torque, in order to maintain a constant torque as demanded.
- *Dynamic reference torque setting during load perturbation (Case C)*: This demonstrates a worst case scenario where disturbance torque is applied dependent on the perturbed speed, resulting from the alternating shaft torque. In comparison to *Case A* due to the simultaneous increase in m_g , the difference between maximum of m_a and m_t is small.

Based on the measurements obtained from experiments described above and illustrated in Fig.6, system dynamic response has been preserved in terms of magnitude of compared signals and the corresponding phase shift taking place. The resulting frequency responses are composed as shown in Fig.7, with respect to signal paths illustrated in the block diagram in Fig.8. Here, the underlying drive system is represented by A , while HiL controller includes K and L as controller and observer, respectively.

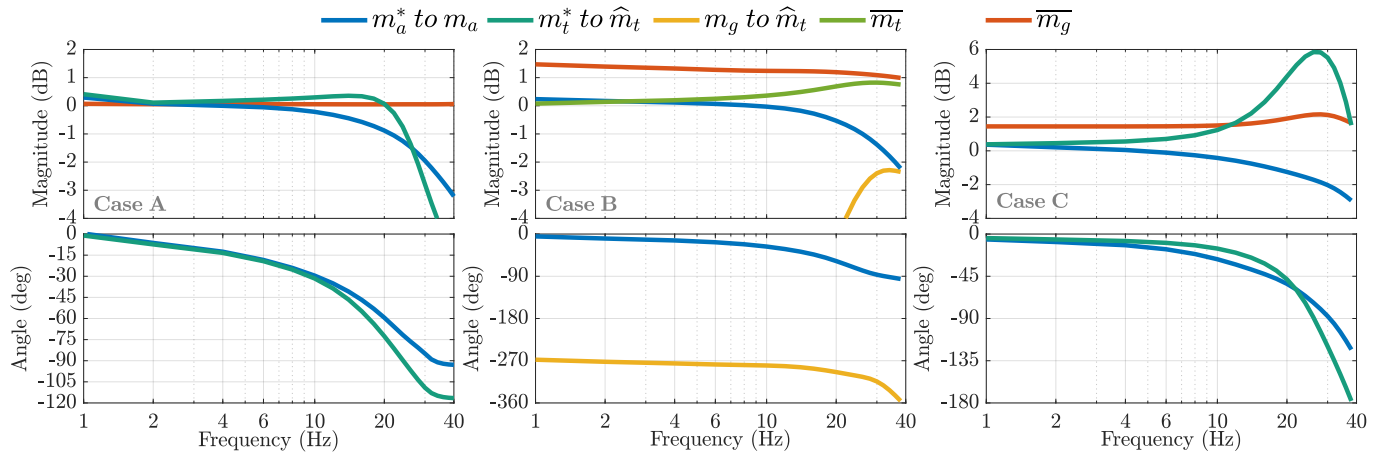


Fig. 7. Complete system frequency response

Furthermore, \mathbf{G} is the power curve implemented on generator side enabling variable torque and speed operation. P_{01} and P_{02} here designate sections of the plant introduced in section 3. Overall, the system response demonstrated here does not only include inherent dynamics of the HiL controller, but also that of the underlying drive control as well as the effect of dead-times due to communication in the distributed drive system. Moreover, the interaction of active controllers on the motor and generator side is understood in this way. It has to be mentioned that the illustrated curves for \overline{m}_g and \overline{m}_t represent ratio of the peak value with respect to a constant reference, illustrating how large magnitude of the alternating signal is. For the case of \overline{m}_g , mean value of m_g is the reference, and \overline{m}_t is obtained considering \hat{m}_t as the reference signal.

According to the measurements obtained as summarized in Fig.7, the drive system provides air-gap torque with a control bandwidth of 40 Hz (m_a^* to m_a), while introducing a phase shift of up to 90 degrees. The linear increase observed in phase shift up to 10 Hz, demonstrates clearly the effect of dead-time reducing the resulting phase margin. In the presence of this actuator response, bandwidth of the HiL controller in terms of reference following is observed to be as high as 30 Hz (m_t^* to \hat{m}_t) with a phase margin of 60 degrees, under the nominal condition defined for Case A. This is well beyond the demanded dynamic induced from a rotor, known to require up to 10 Hz. Therefore, sufficient reserve for control action is demonstrated to be maintained.

On the other hand, for an evaluation of the disturbance rejection performance, frequency response for Case B is illustrated in Fig.7 with respect to the alternating input m_g . It can be clearly seen that the system is immune to the input disturbance in a frequency range up to 8 Hz. Overall, the influence of disturbance on the output (m_g to \hat{m}_t) is stronger in higher frequencies, leading the output to reach 0.8 dB of its average at a frequency of 30 Hz. This indicates

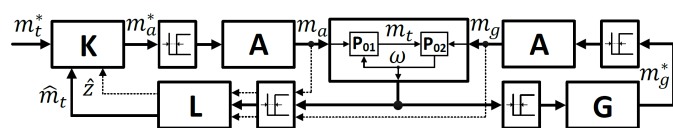


Fig. 8. Simplified block diagram of the system in the back-to-back test configuration

the impact of actuator response taking effect in a lagged manner, leading to a delayed compensation of the alternating load. This effect is as a consequence of the delay taking effect due to communication dead-times in the underlying distributed drive control system, as well as the magnetization time constant of the electrical machine. This effect holds true, although the drive provides torque as fast as 1% in a milli second, after a communication dead-time of 3 milli seconds, both leading to an overall bandwidth of 40 Hz as described previously.

System response during a worst case scenario is demonstrated in the bode diagram corresponding to Case C, being a combination of conditions for Case A and B. In this case the load alternates in correlation with the actual speed, being itself perturbed due to the alternating shaft torque. This has led to a reduction of the control bandwidth and an oscillatory response around the desired edge frequency. This is mainly due to the positive feedback formed through the additional loop from ω to m_g . The mentioned effect is understood when comparing \overline{m}_g in all above bode diagrams, demonstrating an increased magnitude of load oscillations in higher frequencies during operation in Case C. This effect is considered to be the interaction taking place between active controllers on the motor and generator side, working against each other. It is also due to the mentioned reason that undesired oscillations occur at higher frequencies, being independent of any mechanical vibrations. This is essential for understanding of system behaviour during tests with a commercial DUT, since up to now most of the focus in the literature has been on damping of mechanical vibrations, demonstrated here not to be the only cause of possible oscillations.

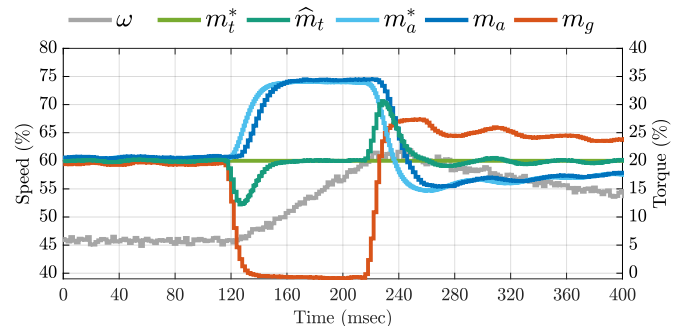


Fig. 9. System response to 20% torque dip

For further clarification on the impact of delay on system response, the illustrated test in Fig.9 is performed by exerting a dramatic step load drop. Here, a torque dip down to zero is applied, while being at a constant operation of 20 % torque at a speed of 45 %. The system response here demonstrates once again the control to maintain steady-state accuracy. However, the response during this transient event indicates deviation of the output torque as a result of the lagged drive response, as mentioned previously. Furthermore, a comparison of the results for both of the implemented control systems demonstrate similar results. This is in fact the case, although the implemented feedback-feedforward controller adjusts the actuating variable more aggressively. In addition, it has been observed that the required effort for parametrization and tuning of both controllers are identical in practice, based on the initial experience from simulations. Nevertheless, the steady state accuracy is more sensitive to model parameters for the feedback-feedforward controller, in comparison with the H-infinity controller which provides robustness in this regard.

5. CONCLUSION

The measurement results demonstrate a high steady-state accuracy and a closed-loop system performance with dynamics as high as 30 Hz. This is achieved by taking advantage of the direct drive machines as well as the effective drive train control, both enabling high dynamics for the system with a high inertia and a minimal measurement availability. Furthermore, a comparison of experiment results for both control systems implemented does not distinguish any significant difference. Although the feedback-feedforward controller adjusts the actuating variable more aggressively in comparison with the H-infinity controller, but it is the lagged drive response that leads to similar response for both cases. The parametrization and tuning effort for both controllers are also observed to be identical, however, the steady-state accuracy is more sensitive to model parameters in the case of the feedback-feedforward controller. In addition, experimental results demonstrate a reduction of control bandwidth during transient disturbance events. This is due to the lagged actuator response, as a result of the existing dead-times in the control loop mainly in the underlying distributed drive control system, and also the magnetization time constant of the electrical machine. Moreover, it is demonstrated that the mentioned impact of time delay could cause torque and speed oscillations not being related to any mechanical vibrations. Overall, the performance evaluation achieved here is essential for system understanding during tests with a commercial specimen. More importantly, the implemented control system provides stability and robustness in the presence of dead-times and actuator limitations, and demonstrates an accurate and effective performance.

ACKNOWLEDGEMENTS

The work presented in this paper is carried out as part of the project CertBench, funded by German Federal Ministry for Economics Affairs and Energy (BMWi), supported by the Project Management Juelich (PTJ). Furthermore, the authors would like to acknowledge Mr. Gabriele Curioni for the support during test execution.

REFERENCES

- Feja, P. and Huhn, M. (2019). Real-time simulation of wind turbines for hil-testing with mowit. Wind Energy Science Conference, EAWE.
- FGW (2018). *Technical guidelines for power generating units and systems*, chapter TG3 - determination of the electrical characteristics of power generating units and systems. Rev. 25. FGW e.V. Foerdergesellschaft Windenergie und andere Erneuerbare Energien.
- Fischer, B. and Jassmann, U. (2017). A general framework for a control-based design of power and mechanical hardware-in-the-loop systems. volume 50 of 1, 10957–10963. 20th IFAC World Congress, Elsevier.
- Fischer, B., Mehler, C., Zuga, A., and Shan, M. (2016). Control design for mechanical hardware-in-the-loop operation of dynamometers for testing full-scale drive trains. *Wind Energy*, 19(10), 1889–1901.
- IEC (2019). *International standard IEC 61400*, chapter wind energy generation systems - Part 21-1: measurement and assessment of electrical characteristics - wind turbines. International Electrotechnical Commission (IEC).
- Jassmann, U. (2018). Hardware-in-the-loop wind turbine system test benches and their usage for controller validation. Dissertation, Aachen, Germany.
- Jassmann, U., Mehler, C., Roettgers, H., Santjer, F., Brennecke, M., Abdul, B., and Abel, D. (2019). Certbench: on the status of certifying electrical properties of wind turbines on hardware-in-the-loop system test benches. Conference for Wind Power Drives (CWD).
- Leisten, C., Jassmann, U., Balshuesemann, J., and Abel, D. (2018). Model predictive speed control of a wind turbine system test bench. volume 51 of 32, 349–354. 17th IFAC Workshop on Control Applications of Optimization (CAO), Elsevier.
- Neshati, M., Curioni, G., Karimi, H.R., and Wenske, J. (2017). H-∞ drive train control for hardware-in-the-loop simulation with a scaled dynamometer test bench. IECON 2017 - 43rd Annual Conf. of the IEEE Industrial Electronics Society, IEEE.
- Neshati, M., Zuga, A., Jersch, T., and Wenske, J. (2016). Hardware-in-the-loop drive train control for realistic emulation of rotor torque in a full-scale wind turbine nacelle test rig. European Control Conference (ECC), IEEE.
- Neshati, M., Zuga, A., and Mehler, C. (2019). Hardware-in-the-loop framework with emulation of rotor dynamics for electrical certification on a nacelle system test bench. Conference for Wind Power Drives (CWD).
- Schkoda, R., Fox, C., Hadidi, R., Gevorgian, V., Wallen, R., and Lambert, S. (2016). Hardware-in-the-loop testing of utility-scale wind turbine generators. Technical Report, NREL.
- Zhang, H., Wenske, J., Reuter, A., and Neshati, M. (2020). Proposals for a practical calibration method for mechanical torque measurement on the wind turbine drive train under test on a test bench. *Wind Energy*, 23(4), 1048–1062.